

Effects on Ash Chemistry when Co-firing Municipal Sewage Sludge and Wheat Straw in a Fluidized Bed: Influence on the Ash Chemistry by Fuel Mixing

Nils Skoglund,^{*,†} Alejandro Grimm,[‡] Marcus Öhman,[‡] and Dan Boström[†]

[†] Thermochemical Energy Conversion Laboratory, Department of Applied Physics and Electronics, Umeå University, SE-901 87 Umeå, Sweden

[‡] Energy Engineering, Department of Engineering Sciences and Mathematics, Luleå University of Technology, SE-971 87 Luleå, Sweden

ABSTRACT: Municipal sewage sludge (MSS) is of interest for co-combustion with problematic fuels, such as agricultural residues, because of its high content of inorganic elements, which may improve combustion properties of such problematic fuels. Ash transformation when co-combusting MSS with the agricultural residue wheat straw was examined using a bench-scale bubbling fluidized bed (5 kW). Wheat straw pellets were combusted with MSS in both a co-pelletized form and co-firing of separate fuel particles. This was performed to examine whether there is any advantage to either approach of introducing MSS together with a problematic fuel. Co-combusting wheat straw with MSS changed the bed agglomeration characteristics from being caused by the formation of low-temperature melting potassium silicates in the fuel ash to being caused by a higher temperature melting bed ash. This shift in ash chemistry had a significant positive effect on the initial defluidization temperature. The cyclone ash and fine particulate matter changed from being dominated by alkali in general and alkali chlorides in specific to an increased phosphate and sulfate formation, which reduces the risk of alkali-related fouling and corrosion. The influence of aluminosilicates may also play a role in the improvement of fuel ash behavior.

INTRODUCTION

The discussion whether cultivable areas should be used for food production or production of biomass suitable for green energy conversion has today faded in intensity, and food production is considered more important when only one type of land use is discussed. With the increase of the use of agricultural residues from food production in energy conversion, land use may become more efficient. These agricultural residues typically contain relatively large amounts of alkali compared to woody biomass,^{1,2} which has been shown to be a source of boiler operational problems, such as deposit formation, bed agglomeration, and slagging during thermal energy conversion.^{3–10} Such problems may be remedied to some extent by changing the fuel composition with respect to its inorganic content.^{5,6,8–16} This change in fuel composition can be made using other types of biomass,^{4,6,8,10,17} chemical additives,^{8,9,11,14,15} or other waste stream resources together with the agricultural residues in a thermal energy conversion process.

Municipal sewage sludge (MSS) is an example of such a waste stream resource that may be of interest in combustion applications, together with agricultural residues.^{18,19} A summary of analyses made by 47 different sewage sludges from Sweden²⁰ shows that MSS typically contains large amounts of P, S, and Si, elements that have been shown to improve combustion properties of problematic fuels.^{8,16} Co-firing MSS with biofuels originating from agriculture may improve the combustion behavior of such biomasses, effectively decreasing operational problems.^{18,21} The alkali content is typically low in MSS. Its content of potentially harmful elements is relatively high, which may be remedied by co-combustion with biomass that contains low amounts of, e.g., cadmium, copper, and lead. MSS has a high

ash content and a fairly high heating value, which mostly varies with its water content.

Introducing a small share of sewage sludge together with a problematic fuel may provide several positive effects.^{18,19} The most interesting aspects are improving combustion properties without making large sacrifices in energy content while effectively diluting potentially harmful elements present in the sewage sludge. The ashes produced by such co-combustion may assist in improving phosphorus recycling within food production because some of the phosphorus present in MSS comes from food.^{22–24} Phosphorus is an important nutrient that is a major component in fertilizers; therefore, it would be beneficial to capture some of the phosphorus introduced to cultivated areas in ash fractions that could be used again in the same or other areas as fertilizing agents.

Wheat straw (WS) is an agricultural waste product that is considered a problematic biofuel in combustion applications.^{4,8,9,13,25} The high alkali content in WS leads to the formation of low-melting compounds, typically silicates, which cause operational problems.^{16,25} The formation of particles containing alkali chloride is also common during combustion of WS, which increases the risk of fouling and corrosion. It is possible that these ash-related issues could be resolved by co-combustion with MSS.

Fluidized bed technology is a suitable method to examine effects of such co-combustion.²⁵ The relatively long residence

Special Issue: Impacts of Fuel Quality on Power Production and the Environment

Received: April 12, 2013

Published: July 18, 2013

time and turbulence in the bed promote reactions in the inorganic fuel content. Another factor that may impact the reaction rates is how the fuels are mixed. For this reason, it is interesting to compare co-pelletized fuel particles and separate fuel particles. The process temperature is also lower and more uniform in a fluidized bed than in grate-fired systems, which is advantageous when studying problematic fuels.

The aim of this study is to determine bed agglomeration characteristics and fine particle formation during co-combustion of WS and MSS introduced by co-pelletizing and separate fuel particles. These phenomena will be discussed from the perspective with ash transformation processes in mind.

MATERIALS AND METHODS

Bed Material and Fuels. The bed material used in fluidized-bed experiments was quartz sand (>98% SiO₂) sieved to a grain size fraction of 200–250 µm. The two fuels used in this study were MSS, which had been precipitated with iron(II) sulfate, and WS, representing a typical problematic fuel. They were mixed as 90:10 (w/w, %) WS and MSS in the co-pelletized (co-p) mixture and co-fired as separate fuel particles (sfp), with all fuels and mixtures fired as 6 mm pellets. This mixing ratio was chosen on the basis of the molar ratio of potassium over phosphorus and sulfur, which indicates the amount of anion formers available to capture potassium in compounds other than chlorides and silicates. The fuel ash composition for raw materials and mixtures is provided in Table 1.

Table 1. Composition of the Fuels Used in This Study

	WS	WS + MSS (90:10, w/w, %) ^a	MSS
w/w, % of Dry Substance			
ash content	5.7	9.3	41.7
K	1.25	1.2	0.37
Na	0.03	0.04	0.17
Ca	0.40	0.61	2.5
Mg	0.10	0.14	0.51
Al	0.006	0.24	2.3
Fe	0.005	0.77	7.7
Si	0.80	1.1	3.7
P	0.13	0.54	4.2
S	0.19	0.31	1.4
Cl	0.26	0.23	<0.05
Molar Ratios			
K/Si	1.1	0.77	0.07
K/(P + S)	3.2	1.1	0.05
K/Al	152	3.4	0.11

^aCalculated values.

Bed Agglomeration Experiments. A bench-scale bubbling fluidized bed (see Figure 1) was used for the combustion experiments. The fluidized bed has an inner diameter of 100 mm at the 1% perforated (90 holes) stainless-steel air distribution plate. The freeboard section has an inner diameter of 200 mm, and the total height of the fluidized bed is 2 m. The experiments were divided into two parts: a combustion period, followed by a bed agglomeration test when applicable. The combustion period lasted for 8 h or until bed defluidization occurred for WS, and its mixtures with MSS was only fired for 90 min because of its very high ash content. During this time, the oxygen level as determined using a λ probe was kept at 8–10%, with a fluidization velocity of about 10 times the minimum fluidization velocity (~1 m/s). The bed temperature was kept at approximately 730 °C for WS, while the mixtures and MSS were fired with a bed temperature of approximately 800 °C at an effect of ~5 kW. The freeboard section of the furnace was kept at the same temperature as the bed using electrical heaters. A deposit probe cooled to ~450 °C was introduced in the freeboard to simulate a heat exchanger tube. Cyclone ash (>10 µm) was collected after cooling. Particulate matter sampling

was made using two methods: a total dust filter and a low-pressure impactor from Dekati, Ltd. (DLPI). A bed sample was collected after the combustion period before starting the agglomeration tests.

The defluidization temperature was determined by monitoring the upper and lower bed pressures and temperatures. The resulting data were processed in principal component analysis (PCA) to determine at which temperature the differential bed pressure shifted heavily, which was used as the indicator for initial bed defluidization. If bed defluidization had not occurred during the combustion period, the fuel feeding was stopped and propane was fired to keep O₂ at 8–10%. Using electrical heaters, the bed temperature was slowly raised (~3 °C/min) until defluidization could be observed. A bed sample was also collected after the bed has cooled to determine the bed particle neck characteristics. The reproducibility of the initial defluidization temperature measured with this method has previously been determined to be ±5 °C.²⁶

Chemical Characterization. Elemental and morphological analyses of the samples (bed ash/agglomerates and impactor samples) were made using a Philips model XL30 scanning electron microscope (SEM) combined with an energy-dispersive X-ray spectrometer (EDS). Powder X-ray diffraction (XRD) was used to determine which compounds were formed in the cyclone ash, deposits, and particulate matter. Diffraction data were collected using continuous scans on a Bruker d8 Advance instrument in θ–θ mode with Cu Kα radiation, where the optical configuration consisted of a primary Göbel mirror and a Väntec-1 detector. The initial phase identification was made using Bruker software and the PDF-2 database.²⁷ Subsequent semi-quantitative analysis of crystalline material was performed with Rietveld refinement using structures from Inorganic Crystal Structure Database (ICSD).²⁸

RESULTS

The observed initial bed defluidization temperatures are shown in Table 2. To determine the degree of interaction between fuel ash and bed particles, as well as bed agglomeration mechanisms, SEM–EDS images, such as those shown in Figure 6, were used. For all fuels containing MSS, there was a large amount of large (>1 mm) red fuel ash particles in the bed material that had not interacted with bed grains to any large extent. Such large ash particles constituted the greater part of bed ash for both mixed fuels. XRD analysis of these ash particles for the co-pelletized fuel mix shows that hematite is responsible for the red color and alkali is found in phosphates, sulfates, and silicates (see Table 3). The quartz content is mainly bed material included in these large ash particles.

For WS, bed grains were found to only have discontinuous outer coating layers in general. Even though the bed grains displayed discontinuous outer coating layers in general, bed grains in agglomerates showed both inner and outer layer reaction layers, with a fuel ash particle acting as an adhesive. Fuel ash particles adhering to bed grains dominated agglomerate necks. In the co-combustion cases, separate fuel particles formed agglomerates similar to those found for WS but to a lesser extent. The co-pelletized fuel mixture did not show the same agglomeration interaction; the outer coating layers on bed grains were scarce; and there were no agglomerate necks found, suggesting that the bed ash is responsible for defluidization. Bed grains from MSS combustion were similar to those found for the co-pelletized fuel with almost no outer layer formation.

Ash particles forming necks (WS) and ash particles found in the bed (fuel mixtures and MSS) were analyzed with SEM–EDS (see Figure 2). The values shown are averages of 10 different spot and area analyses of bed agglomerates and particles. Silicon has been omitted because of some inclusion of bed material. WS ash was dominated by potassium silicates, while the fuel mixtures and MSS displayed a more complex composition. Spot analysis of bed ash from fuel mixture combustion showed that the phosphorus

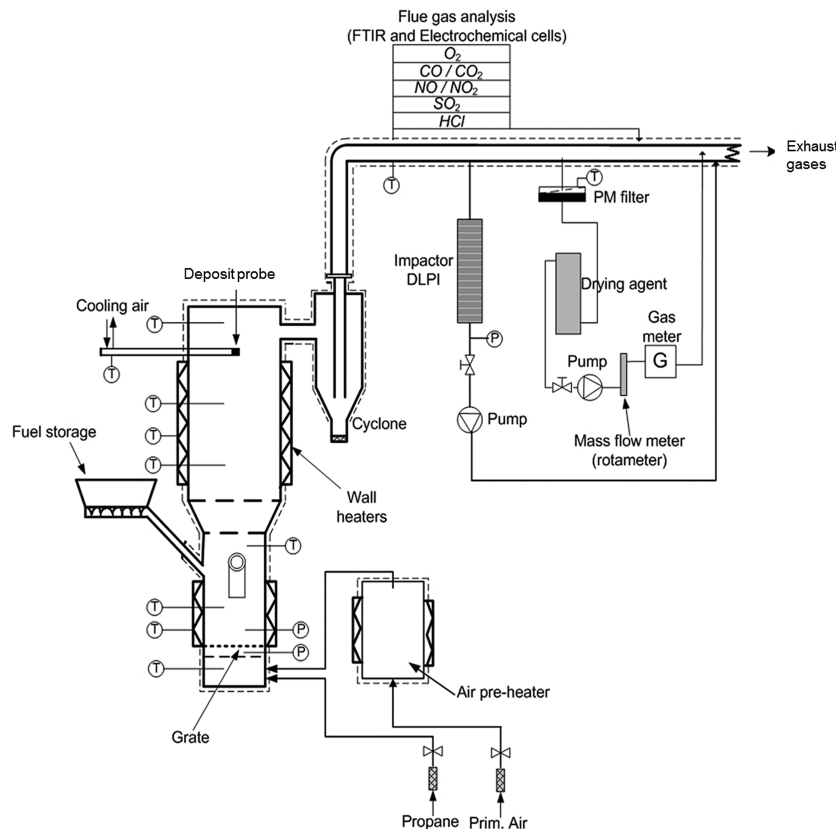


Figure 1. Schematic image of the bench-scale bubbling fluidized-bed reactor. Fuel feed and sampling points are indicated in the image.

Table 2. Initial Defluidization Temperatures (IDFs) for Fuels and Mixtures^a

fuels	IDF (°C)
WS	750
WS + MSS (co-p)	960
WS + MSS (sfp)	970
MSS	>1050

^aFuel mixtures are abbreviated as co-p (co-pelletized) and sfp (separate fuel particles).

Table 3. Compounds Identified in Large Bed Ash Particles^a

compound	w/w, %
Ca ₉ KMg(PO ₄) ₇	18
K ₂ SO ₄	6
KAlSi ₂ O ₆	20
KAlSi ₃ O ₈	3
Ca _{0.25} Na _{0.75} AlSi ₃ O ₈	7
SiO ₂	28
Fe ₂ O ₃	18

^aCompounds formed in large bed ash particles (>1 mm) during combustion of co-pelletized WS and MSS. Results from the semi-quantitative Rietveld analysis are provided as w/w, %.

content was related to a higher content of calcium and that some sulfur had stayed in the bed. Alkali levels were usually higher when the silicon content also reached higher levels in the ash particle, especially for WS and the mixture with separate fuel particles.

Cyclone ash and deposition probe rings (wind side and lee side, respectively) were analyzed with SEM-EDS to determine elemental composition (see Figures 3–6). The deposition

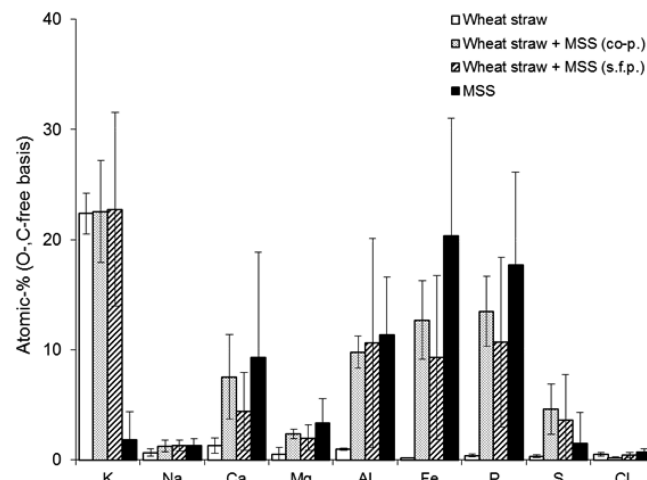


Figure 2. Elemental composition of bed agglomerate necks (WS) and bed ash particles (all fuels). Si was omitted because of the inclusion of bed material.

growth rate on the cooled probe rings is shown in Table 4. XRD analysis was made to determine which phases were present, and Rietveld calculations were used to provide a semi-quantitative analysis of the phases identified (see Table 5). The deposits on probe rings from WS experiments (wind side) and MSS experiments (lee side) contained too little material to admit analysis. The shift from lee-side deposits to a more differentiated deposit formation may indicate that MSS addition to WS could facilitate soot blowing.

The particle mass size distribution of particulate matter was determined using a low-pressure impactor (see Figure 7).

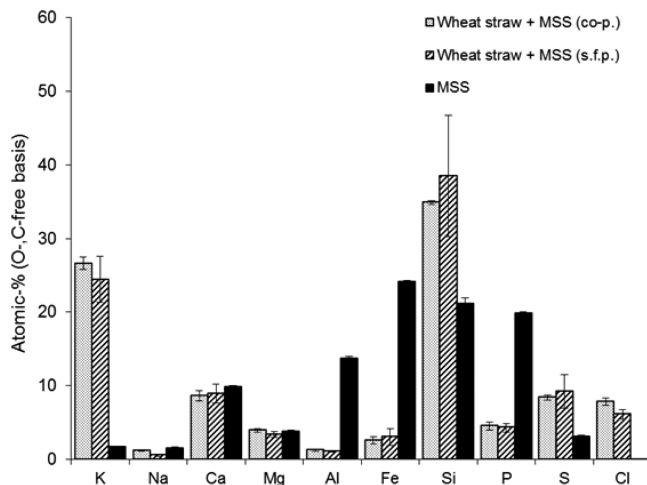


Figure 3. Elemental composition of deposits from the deposition probe wind side on a carbon- and oxygen-free basis. WS did not provide enough material for analysis.

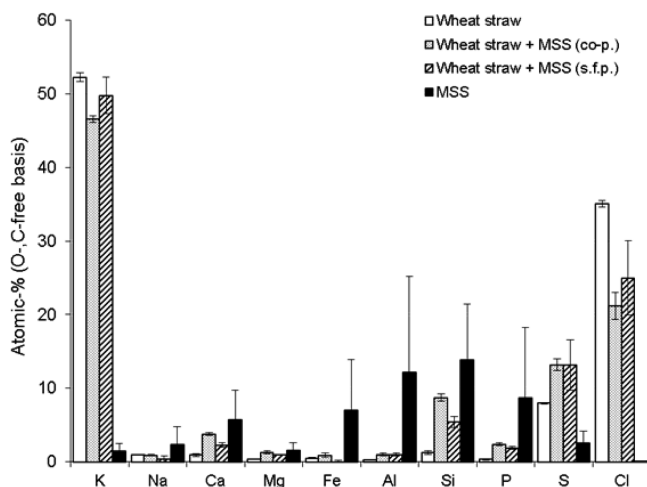


Figure 4. Elemental composition of deposits from the deposition probe lee side on a carbon- and oxygen-free basis.

The coarse ($>1 \mu\text{m}$) and fine ($<1 \mu\text{m}$) mode fractions of particulate matter were submitted to subsequent analyses in SEM-EDS and XRD.

Results are shown in Figures 8 and 9 and Table 6. In some cases, the amount of sample was too small to admit XRD analysis, which is marked as NA in Table 6, and it is the reason why the MSS fine mode fraction was not analyzed using SEM-EDS.

DISCUSSION

The agglomeration tendencies of WS are greatly reduced by co-combustion with MSS (see Table 2). This suggests that even if MSS has a lower heating value than that of WS, it may be beneficial to use it for co-combustion with WS or other problematic fuels in fluidized-bed boilers because a higher system temperature could be employed. The distribution of ash-forming elements on a macro- and microscale influences ash chemistry in ways that can be considered decisive for the reactivity because this distribution affects reaction rates and, thereby, the possibility of reaching chemical equilibrium. When the different approaches are compared to co-combustion, i.e., co-pelletizing or co-firing of separate fuel particles, it can be

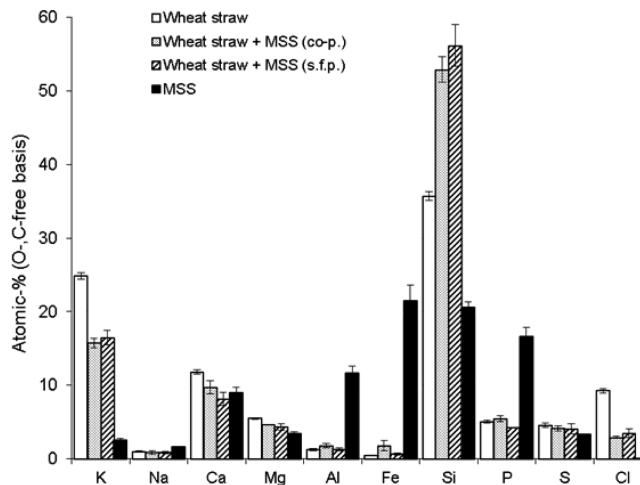


Figure 5. Elemental composition of cyclone ash ($>10 \mu\text{m}$) on a carbon- and oxygen-free basis.

seen that there is no significant difference in the initial defluidization temperature.

The classification system for bed agglomeration mechanisms suggested^{29,30} and further developed in the literature^{8,31} can be applied in this study using results from SEM-EDS images of bed material. Bed agglomeration during WS combustion occurs through potassium silicate formation by reaction of potassium in a gaseous or aerosol phase with silicon introduced with the fuel. This reaction yields low-temperature melting potassium silicates that act as an adhesive between bed grains, which promotes agglomeration. The interaction between bed grains and alkali introduced is limited in this case, in agreement with the literature;^{8,25} therefore, the agglomeration mechanisms can be classified as direct adhesion of bed particles by partly molten-ash-derived potassium silicate particles/droplets.⁸ For MSS, there were no agglomerates formed during combustion and the quartz bed grains exhibited almost no interaction with the fuel ash even after the agglomeration test. For the two fuel mixtures, there was a slight difference: the co-pelletized fuel was more similar to MSS (scarce outer layer coatings dominated and agglomerate necks), while the separate fuel particles formed agglomerate necks similar to those found in WS with both an inner and outer reaction layer on bed grains at the formed agglomerates. This difference is likely due to physical restraints affecting reaction rates, where ash-forming elements in the co-pelletized fuel have a short distance to travel before they can interact. Bed ash particles sticking together when their melting temperature is reached is therefore responsible for bed agglomeration. In the case of separate fuel particles, the ash-forming elements from WS pellets may have time to interact with bed grains before ash from a MSS pellet is close enough to mitigate this interaction. Once an inner reaction layer has formed on quartz bed grains, it is likely that an outer reaction layer containing Ca will form.

The large variation in elemental analysis data for bed agglomerates and bed material in Figure 2 shows that the bed ash particles were heterogeneous, where some of the ash formed when co-firing as separate fuel particles behaved similarly to WS, something that was not observed for the co-pelletized fuel. The bed ash formed for co-pelletized fuel seems to have a slightly higher content of phosphorus, calcium, and iron than for the co-fired mixture. This difference is not large when including area analysis in the data; using spot analysis, this correlation seemed to exist.

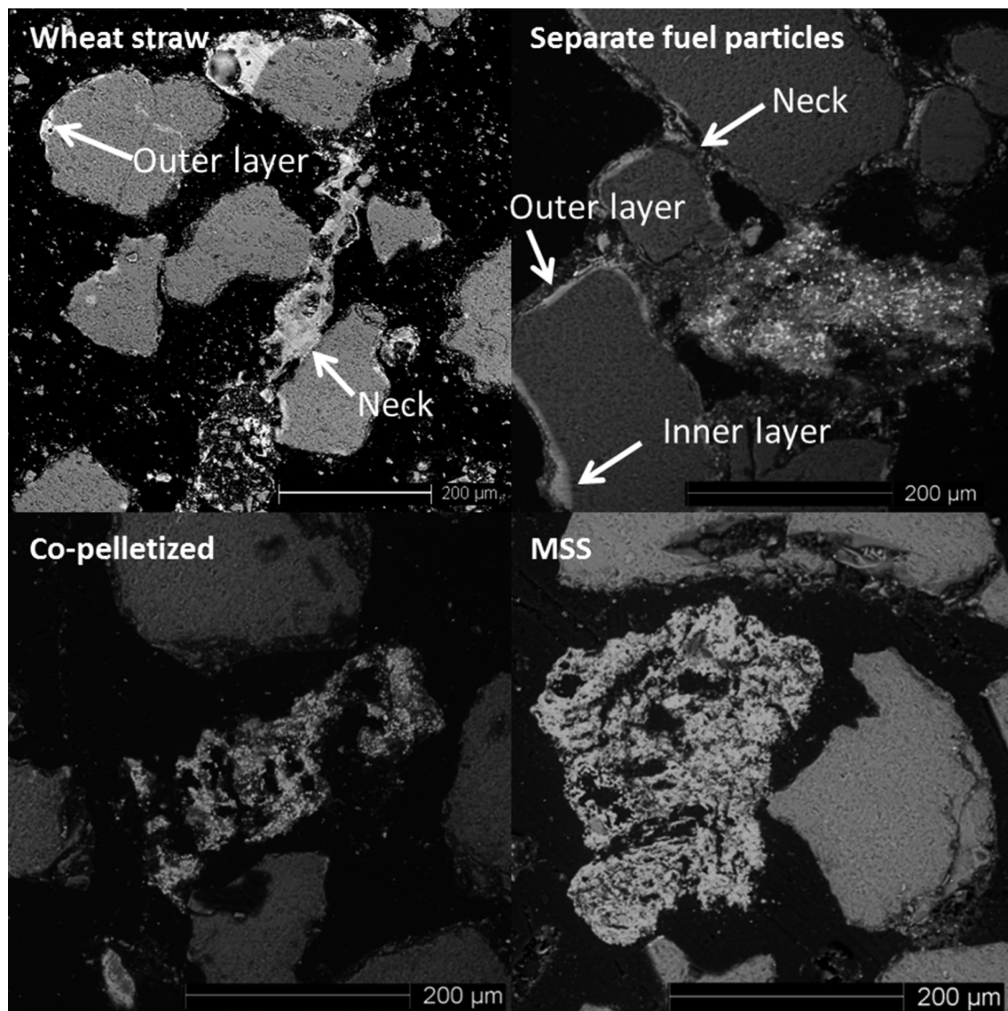


Figure 6. SEM images of typical cross-sections of bed material after agglomeration tests. WS and the separate fuel particle experiments display similarities in the agglomerates found. For the co-pelletized fuel and MSS, agglomerate necks could not be observed. Bed ash particles are the brighter particles, and quartz bed grains are the dimmer, larger particles. Outer layers are the brighter lines surrounding bed grains; inner layers are reaction fronts moving into bed grains; and necks are found where bed ash is interacting with bed grains.

Table 4. Deposition Growth Rate and Total Particulate Matter Emissions^a

fuels	deposition growth (mg cm ⁻² h ⁻¹)	total particulate matter (mg/Nm ³ at 10% O ₂ dg)
WS	0.34	323
WS + MSS (co-p)	0.17	227
WS + MSS (sfp)	0.28	334
MSS	0.11	285

^aParticulate matter emissions were measured after the flue gas passed through a cyclone with a 10 μm cut-off.

This suggests that the method of fuel mixing does affect the reactivity of the fuel ash regarding the ash chemistry. Even though bed ash particles did eventually melt and act as an adhesive for bed grains to form agglomerates that defluidized the bed, this occurred at a considerably higher bed temperature than for WS. This may be related to several components in the fuel ash, where phosphorus, sulfur, and aluminosilicates specifically have been suggested to improve bed performance.^{8,16,32} XRD analysis of large bed ash particles from the co-pelletized fuel suggests that alkali does bond in phosphates, sulfates, and aluminosilicates, while SiO₂, found as quartz, does not react with

alkali to any large extent when more reactive anions are present (see Table 3). The phosphate Ca₉KMg(PO₄)₇ identified in the large ash particles has a structure that allows it to substitute both Ca, K, and Mg for other elements, including iron and sodium. This compound likely contributes to the increased defluidization temperatures for the two fuel mixtures. The presence of K₂SO₄ in bed ash particles shows that the large amount of sulfur introduced with MSS also contributes significantly to improving the ash characteristics. Additionally, the feldspars found are likely to also contribute to a higher defluidization temperature in the fuel mixtures.

Deposit formation rates are significantly lower for MSS compared to WS, and MSS has almost no deposits forming on the lee side of the deposit probe. This is most likely connected to the small amount of fine particulate matter produced, as seen in the impactor curve (see Figure 7), which, in turn, may be related to the low alkali content in MSS. For the fuel mixtures, the co-pelletized fuel creates a noticeably smaller amount of deposits as well as total particulate matter compared to the separate fuel particles. This difference could be due to a higher degree of entrainment of coarse ash in the case of separate fuel particles, a notion that is supported by the similar levels of sub-micrometer particles for both co-pelletized and separate fuel particle

Table 5. Phases Identified with XRD from Cyclone Ash (Cycl), Deposit Probe Ring Wind Side (DPW), and Deposit Probe Ring Lee Side (DPL)^a

	WS			WS + MSS (co-p)			WS + MSS (sfp)			MSS		
	cycl	DPW	DPL	cycl	DPW	DPL	cycl	DPW	DPL	cycl	DPW	DPL
$\text{Ca}_5(\text{PO}_4)_3\text{OH}$	19	NA		15			14					NA
$\text{Ca}_3(\text{PO}_4)_2$				19			11			9		
$\text{CaK}_2\text{P}_2\text{O}_7$										7		
CaSO_4				5	4		1	5		7	8	
CaCO_3							3					
K_2SO_4	45			23	35	52	60	39	61	50		8
$\text{K}_3\text{Na}(\text{SO}_4)_2$				11						2		
KCl	35			65	17	28	40	17	30	50		
SiO_2 (quartz)	1				3	15		3		9	7	
SiO_2 (cristobalite)							11			8		
$\text{Ca}_3\text{Mg}(\text{SiO}_4)_2$												
KAlSiO_4										4		
KAlSi_3O_8										11		
NaAlSiO_4											23	
$\text{K}_2\text{Al}_2\text{Si}_4\text{O}_{12}\cdot 6\text{H}_2\text{O}$										9	8	
$\text{Na}_2\text{Al}_2\text{Si}_3\text{O}_{10}\cdot 2\text{H}_2\text{O}$										5	8	
Fe_2O_3					6			5		29	34	

^aThe probe ring wind side from WS experiments and the probe ring lee side from MSS experiments had too little material to admit analysis. Results from the semi-quantitative analysis are provided as w/w, %. Abbreviations used are co-p for the co-pelletized mixture and sfp for the separate fuel particles.

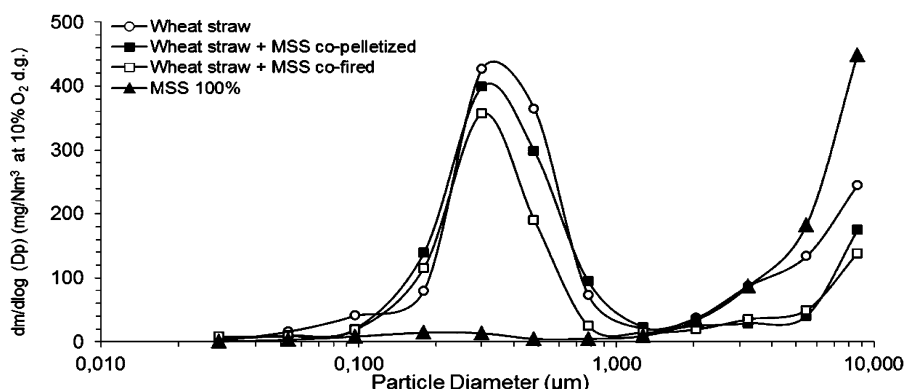


Figure 7. Particle mass size distribution in flue gas during combustion of the fuels and fuel mixtures normalized to 10% O_2 .

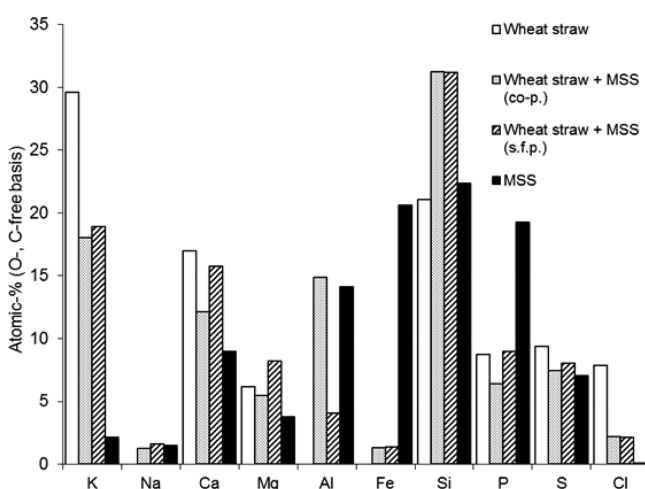


Figure 8. Elemental composition of the coarse mode ($1-10 \mu\text{m}$) fraction from impactor sampling shown as atomic % on a carbon- and oxygen-free basis.

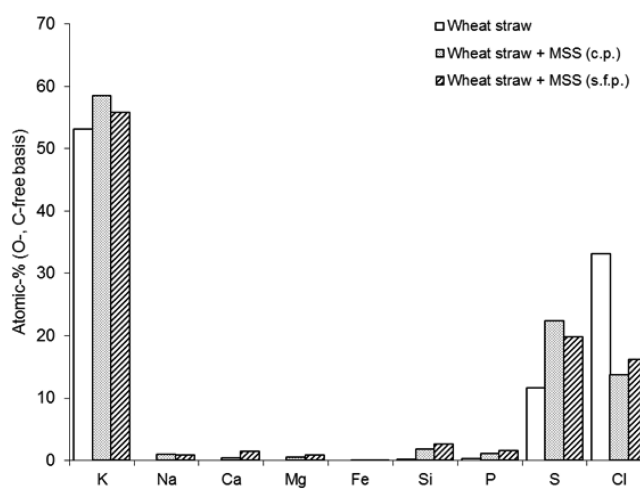


Figure 9. Elemental composition of the fine mode fraction ($<1 \mu\text{m}$) from impactor sampling shown as atomic % on a carbon- and oxygen-free basis. MSS was omitted because the small amount of sample was insufficient for analysis.

Table 6. Phases Identified with XRD in Impactor Coarse Mode (ICM) and Fine Mode (IFM)^a

	WS		WS + MSS (co-p)		WS + MSS (sfp)		MSS	
	ICM	IFM	ICM	IFM	ICM	IFM	ICM	IFM
Ca ₅ (PO ₄) ₃ OH	17		NA				NA	
Ca ₃ (PO ₄) ₂							1	
CaSO ₄							12	
K ₂ SO ₄	52	23			83	88	75	7
K ₃ Na(SO ₄) ₂	2				17	12	25	
KCl	22	77						
SiO ₂ (quartz)							6	
SiO ₂ (cristobalite)								
Ca ₂ Mg(SiO ₄) ₂	7						4	
KAlSi ₃ O ₈							12	
NaAlSi ₃ O ₈							12	
K ₂ Al ₃ Si ₄ O ₁₂ ·6H ₂ O							14	
Na ₂ Al ₂ Si ₃ O ₁₀ ·2H ₂ O							32	
Fe ₂ O ₃								

^aFine mode from MSS experiments contained too little material to admit analysis. Results from the semi-quantitative analysis are provided as w/w, %. Abbreviations used are co-p for the co-pelletized mixture and (sfp for the separate fuel particles.

combustion (see Figure 7). The amount of KCl in the deposits formed on the lee side of the probe rings is reduced slightly, and a smaller amount of material was found on the lee side of probe rings when firing fuel mixtures compared to WS. This suggests that co-combustion may reduce the risk of alkali-related fouling and corrosion. The compounds found in probe ring deposits show that, for MSS, there is little formation of alkali chloride. Further investigation of this relation is required to clarify if there is a point where KCl in deposits is reduced by co-combusting MSS with agricultural residues.

In the cyclone ash, the addition of MSS caused the formation of an increased share of phosphates and sulfates compared to WS combustion. This led to a decrease in the relative amount of KCl found. Hematite (Fe₂O₃) was also formed because of the high content of iron in the MSS. When MSS was fired, the cyclone ash contained some phosphates and sulfates, as well as a high content of hematite and aluminosilicates (zeolites), with some alkali content. The amount of cyclone ash was, however, very small when firing MSS.

The particulate matter emissions differ between the unmodified fuels (see Figure 7). WS combustion yields mostly fine mode particulate matter (<1 μm) but almost no coarse mode particle matter (1–10 μm), while the opposite can be said for MSS combustion. When the co-combustion experiments are compared to the WS, it can be seen that the fine mode particulate matter decreases somewhat, slightly more for separate fuel particles, and the coarse mode decreases. SEM-EDS and XRD analyses show that the composition of the fine particulate matter changes by an increase of silicon, aluminum, and iron, while the relative amount of alkali and chlorine decreases. Particulate matter formed during WS combustion mainly consists of KCl with some K₂SO₄ in the fine mode. This shifted heavily in favor of sulfate formation during co-combustion with MSS. Reducing the amount of alkali chlorides is important to reduce alkali-related fouling. While there is still some KCl formed during combustion of the fuel mixtures in this study, it is evident that sulfur introduced with MSS has a positive effect on particulate matter characteristics. For MSS, the coarse mode in particulate matter mainly contained hematite and various silicates.

Co-combusting a problematic fuel, such as WS, with MSS can be used in fluidized beds to improve fuel performance. Changing the bed agglomeration characteristics from the formation

of low-temperature melting potassium silicates from the fuel ash to a higher temperature melting bed ash has a significant effect on the initial defluidization temperature. The cyclone ash and fine particulate matter change from being dominated by alkali in general and alkali chlorides in specific to an increased phosphate and sulfate formation, which reduces the risk of alkali-related fouling and corrosion. The influence of aluminosilicates may also play a part in improving fuel ash behavior from an operational point of view. Choosing how to mix the fuels will also have an effect on the ash chemistry, where co-pelletizing MSS and WS will cause bed ash to behave more like MSS, while co-firing separate fuels will allow for some of the WS to form alkali silicates. Both methods do however change the fine particulate matter content from chlorides to sulfates, where co-pelletized fuels might be slightly better than co-firing fuels.

CONCLUSION

The results show that co-combustion of problematic straw fuels with MSS may improve the performance of such problematic fuels in fluidized beds. In particular, the following effects were observed: (1) Bed defluidization tendencies were greatly reduced when co-combusting WS and MSS because of a shift in bed agglomeration characteristics from the formation of potassium silicates in the fuel ash with low melting points to the formation of bed ash with a higher melting point. (2) Deposition buildup rates were improved during combustion of the co-pelletized fuel mixture, an effect that was not seen for the separate fuel particles. The amount of KCl on the lee side of deposit probe rings was reduced slightly by the introduction of MSS together with WS. (3) The amount of particulate matter emissions by WS was not reduced to any great extent by co-combustion; however, there was a strong shift from alkali chloride formation for WS toward alkali sulfate formation in the co-combustion experiments, which may decrease the risk of alkali-chloride-related corrosion. (4) Co-pelletizing and co-firing fuels may provide similar benefits for the bed agglomeration temperature, but the effects on ash chemistry are not quite the same, which can be seen in the presence or absence of agglomerate necks and bed-grain-coating layers, as well as changes in particulate matter amount and composition.

AUTHOR INFORMATION

Corresponding Author

*Telephone: +46-72-545-68-01. E-mail: nils.skoglund@umu.se.

Notes

The authors declare no competing financial interest.

ACKNOWLEDGMENTS

The financial support from the Thermal Engineering Research Foundation (Värmefforsk), the Swedish Energy Agency (STEM), the Swedish Research Council (VR), and the National (Swedish) Strategic Research Program Bio4Energy is gratefully acknowledged. The technical support provided by Ulf Nordström during the project is also greatly appreciated.

REFERENCES

- (1) Vassilev, S. V.; Baxter, D.; Andersen, L. K.; Vassileva, C. G. An overview of the chemical composition of biomass. *Fuel* **2010**, *89*, 913–933.
- (2) Vassilev, S. V.; Baxter, D.; Andersen, L. K.; Vassileva, C. G.; Morgan, T. J. An overview of the organic and inorganic phase composition of biomass. *Fuel* **2012**, *94*, 1–33.
- (3) Khan, A. A.; de Jong, W.; Jansens, P. J.; Spliethoff, H. Biomass combustion in fluidized bed boilers: Potential problems and remedies. *Fuel Process. Technol.* **2009**, *90*, 21–50.
- (4) Eriksson, G.; Grimm, A.; Skoglund, N.; Boström, D.; Öhman, M. Combustion and fuel characterisation of wheat distillers dried grain with solubles (DDGS) and possible combustion applications. *Fuel* **2012**, *102*, 208–220.
- (5) Lindström, E.; Sandström, M.; Boström, D.; Öhman, M. Slagging characteristics during combustion of cereal grains rich in phosphorus. *Energy Fuels* **2007**, *21*, 710–717.
- (6) Piotrowska, P.; Zevenhoven, M.; Davidsson, K.; Hupa, M.; Åmand, L. E.; Barisic, V.; Zabetta, E. C. Fate of alkali metals and phosphorus of rapeseed cake in circulating fluidized bed boiler Part 1: Cocombustion with wood. *Energy Fuels* **2010**, *24*, 333–345.
- (7) Silvennoinen, J.; Hedman, M. Co-firing of agricultural fuels in a full-scale fluidized bed boiler. *Fuel Process. Technol.* **2013**, *105*, 11–19.
- (8) Grimm, A.; Skoglund, N.; Boström, D.; Öhman, M. Bed agglomeration characteristics in fluidized quartz bed combustion of phosphorus-rich biomass fuels. *Energy Fuels* **2011**, *25*, 937–947.
- (9) Grimm, A.; Skoglund, N.; Boström, D.; Boman, C.; Öhman, M. Influence of phosphorus on alkali distribution during combustion of logging residues and wheat straw in a bench-scale fluidized bed. *Energy Fuels* **2012**, *26*, 3012–3023.
- (10) Piotrowska, P.; Grimm, A.; Skoglund, N.; Boman, C.; Öhman, M.; Zevenhoven, M.; Boström, D.; Hupa, M. Fluidized-bed combustion of mixtures of rapeseed cake and bark: The resulting bed agglomeration characteristics. *Energy Fuels* **2012**, *26*, 2028–2037.
- (11) Boström, D.; Grimm, A.; Boman, C.; Björnbom, E.; Öhman, M. Influence of kaolin and calcite additives on ash transformations in small-scale combustion of oat. *Energy Fuels* **2009**, *23*, 5184–5190.
- (12) Piotrowska, P.; Zevenhoven, M.; Davidsson, K.; Hupa, M.; Åmand, L. E.; Barisic, V.; Zabetta, E. C. Fate of alkali metals and phosphorus of rapeseed cake in circulating fluidized bed boiler Part 2: Cocombustion with coal. *Energy Fuels* **2010**, *24*, 4193–4205.
- (13) Steenari, B. M.; Lundberg, A.; Pettersson, H.; Wilewska-Bien, M.; Andersson, D. Investigation of ash sintering during combustion of agricultural residues and the effect of additives. *Energy Fuels* **2009**, *23*, 5655–5662.
- (14) Xiong, S. J.; Burvall, J.; Örberg, H.; Kalen, G.; Thyrel, M.; Öhman, M.; Boström, D. Slagging characteristics during combustion of corn stovers with and without kaolin and calcite. *Energy Fuels* **2008**, *22*, 3465–3470.
- (15) Steenari, B. M.; Lindqvist, O. High-temperature reactions of straw ash and the anti-sintering additives kaolin and dolomite. *Biomass Bioenergy* **1998**, *14*, 67–76.
- (16) Boström, D.; Skoglund, N.; Grimm, A.; Boman, C.; Öhman, M.; Broström, M.; Backman, R. Ash transformation chemistry during combustion of biomass. *Energy Fuels* **2012**, *26*, 85–93.
- (17) Eriksson, G.; Hedman, H.; Boström, D.; Pettersson, E.; Backman, R.; Öhman, M. Combustion characterization of rapeseed meal and possible combustion applications. *Energy Fuels* **2009**, *23*, 3930–3939.
- (18) Elled, A. L.; Davidsson, K. O.; Åmand, L. E. Sewage sludge as a deposit inhibitor when co-fired with high potassium fuels. *Biomass Bioenergy* **2010**, *34*, 1546–1554.
- (19) Elled, A.-L.; Åmand, L.-E.; Leckner, B.; Andersson, B.-Å. Influence of phosphorus on sulphur capture during co-firing of sewage sludge with wood or bark in a fluidised bed. *Fuel* **2006**, *85*, 1671–1678.
- (20) Eriksson, J. *Concentrations of 61 Trace Elements in Sewage Sludge, Farmyard Manure, Mineral Fertiliser, Precipitation and in Oil and Crops*; Swedish Environmental Protection Agency: Stockholm, Sweden, 2001; Report 5159.
- (21) Davidsson, K. O.; Åmand, L. E.; Elled, A. L.; Leckner, B. Effect of cofiring coal and biofuel with sewage sludge on alkali problems in a circulating fluidized bed boiler. *Energy Fuels* **2007**, *21*, 3180–3188.
- (22) Adam, C.; Peplinski, B.; Michaelis, M.; Kley, G.; Simon, F. G. Thermochemical treatment of sewage sludge ashes for phosphorus recovery. *Waste Manage.* **2009**, *29*, 1122–1128.
- (23) Pettersson, A.; Andersson, B. A.; Steenari, B. M.; Åmand, L. E.; Leckner, B. Leaching of phosphorus from ashes of co-combustion of sewage sludge and wood. *ASME Conf. Proc.* **2005**, 831–844.
- (24) Pettersson, A.; Åmand, L. E.; Steenari, B. M. Leaching of ashes from co-combustion of sewage sludge and wood—Part I: Recovery of phosphorus. *Biomass Bioenergy* **2008**, *32*, 224–235.
- (25) Lin, W. G.; Dam-Johansen, K.; Frandsen, F. Agglomeration in biofuel fired fluidized bed combustors. *Chem. Eng. J.* **2003**, *96*, 171–185.
- (26) Öhman, M.; Nordin, A. A new method for quantification of fluidized bed agglomeration tendencies: A sensitivity analysis. *Energy Fuels* **1998**, *12*, 90–94.
- (27) International Center for Diffraction Data (ICDD). *The Powder Diffraction File, PDF-2*; ICDD: Newtown Square, PA, 2004.
- (28) Fachinformationszentrum Karlsruhe. *Inorganic Crystal Structure Database (ICSD)*; Fachinformationszentrum Karlsruhe: Karlsruhe, Germany, 1978.
- (29) Brus, E.; Öhman, M.; Nordin, A. Mechanisms of bed agglomeration during fluidized-bed combustion of biomass fuels. *Energy Fuels* **2005**, *19*, 825–832.
- (30) Brus, E. Bed agglomeration during combustion and gasification of biomass fuels: mechanisms and measures for prevention. Licentiate Thesis, Energy Technology and Thermal Process Chemistry, Umeå University, Umeå, Sweden, 2004.
- (31) De Geyter, S. Measures for preventing bed agglomeration using ash reaction chemistry. Licentiate Thesis, Department of Applied Physics and Electronics, Umeå University, Umeå, Sweden, 2008.
- (32) Åmand, L. E.; Leckner, B.; Eskilsson, D.; Tullin, C. Deposits on heat transfer tubes during co-combustion of biofuels and sewage sludge. *Fuel* **2006**, *85*, 1313–1322.